On propagation failure in one- and two-dimensional excitable media

Georg A. Gottwald[a)]
School of Mathematics and Statistics, University of Sydney, Sydney, NSW 2006, Australia

Lorenz Kramer[b)]
Physikalisches Institut, Universität Bayreuth, Universitätstraße 30, D-95440 Bayreuth, Germany

(Received 13 January 2004; accepted 23 May 2004; published online 16 September 2004)

We present a nonperturbative technique to study pulse dynamics in excitable media. The method is used to study propagation failure in one-dimensional and two-dimensional excitable media. In one-dimensional media we describe the behavior of pulses and wave trains near the saddle node bifurcation, where propagation fails. The generalization of our method to two dimensions captures the point where a broken front (or finger) starts to retract. We obtain approximate expressions for the pulse shape, pulse velocity, and scaling behavior. The results are compared with numerical simulations and show good agreement. © *2004 American Institute of Physics.*
[DOI: 10.1063/1.1772552]

Excitable media are often found in biological and chemical systems. Examples of excitable media include electrical waves in cardiac and nerval tissue,[1,2] cAMP waves in slime mold aggregation,[3] and intracellular calcium waves.[4] Excitable media support localized pulses and periodic wave trains. In two dimensions rotating vortices (or spirals) are possible.[5] The critical behavior of pulses, wave trains, and spirals, i.e., propagation failure, is often associated with clinical situations. The study of spiral waves is particularly important as they are believed to be responsible for pathological cardiac arrhythmias.[6] Spiral waves may be created in the heart through inhomogeneities of the properties of the cardiac tissue. We investigate critical behavior relating to these three wave types. We develop a nonperturbative test function method which allows to study the bifurcation behavior of critical waves. In particular, we study under what conditions a broken front will sprout and develop into a spiral wave or retract. Analytical formulas for the growing velocity of a broken front are given. For wave trains we provide a time dependent extension which supports a Hopf bifurcation which is also observed in numerical simulations of excitable media. This seems to be related to alternans,[7,8] which also are discussed in the context of cardiac electric pulse propagation. The methods and results are general, and can be applied to other excitable media.

I. INTRODUCTION

Many chemical and biological systems exhibit excitability. In small [zero-dimensional (0D)] geometry they show threshold behavior, i.e., small perturbations immediately decay, whereas sufficiently large perturbations decay only after a large excursion. One-dimensional (1D) excitable media support traveling pulses, or rather, periodic wave trains ranging in wavelength L from the localized limit $L\to\infty$ to a minimal value L_c. Pulses and wave trains are best known from nerve propagation along axons. In two dimensions (2D) one typically observes spiral waves. Spirals have been observed for example in the autocatalytic Belousov–Zhabotinsky reaction,[5] in the aggregation of the slime mold dictyostelium discoideum,[3] and in cardiac tissue.[2]

For certain system parameters the propagation of pulses, wave trains or the development of spiral waves may fail (see for example Refs. 9 and 10). The analytical tools employed to describe these phenomena range from kinematic theory,[11,12] asymptotic perturbation theory[13–15] to dynamical systems approaches.[16,17] However, no theory exists which describes propagation failure using only equation parameters, and which reproduces the behavior close to the bifurcation point. For example, asymptotic perturbation theory fails to describe the square-root scaling behavior of the amplitude and the pulse velocity with respect to the bifurcation parameter at the bifurcation point. In kinematic theory results are not given entirely in terms of the system parameters. In this paper we develop a nonperturbative method to study propagation failure and compare the results with numerical simulations.

Most theoretical investigations are based on coupled reaction-diffusion models. We follow this tradition and investigate a two-component, two-dimensional excitable medium with an activator u and a nondiffusive inhibitor v described by

$$\partial_t u = D\Delta u + \mathcal{F}(u,v), \quad \mathcal{F}(u,v) = u(1-u)(u-u_s-v),$$
$$\partial_t v = \epsilon(u-av). \tag{1}$$

This is a reparametrized version of a model introduced by Barkley.[18] We expect our method to be independent of the particular model used. Note that the diffusion constant D is not a relevant parameter as it can be scaled out by rescaling the length.

This model incorporates the ingredients of an excitable system in a compact and lucid way. Thus, for $u_s>0$ the rest

a)Electronic mail: gottwald@maths.usyd.edu.au
b)Electronic mail: lorenz.kramer@uni-bayreuth.de

state $u_0=v_0=0$ is linearly stable with decay rates $\sigma_1=u_s$ along the activator direction and $\sigma_2=\epsilon a$ along the inhibitor direction. Perturbing u above the threshold u_s (in 0D) will lead to growth of u. In the absence of v the activator would saturate at $u=1$ leading to a bistable system. A positive inhibitor growth factor ϵ and $a>0$ forces the activator to decay back to $u=0$. Finally, also the inhibitor with the refractory time constant $(\epsilon a)^{-1}$ will decay back to $v=0$. For $a>1/(1-u_s)$ the system is in zero-dimensional systems no longer excitable but instead bistable. This relaxation behavior in the 0D system for superthreshold perturbations gives rise to pulse solutions in the 1D (and 2D) case. The relaxation mechanism mediated by the inhibitor forces the pulse solution to decay in its back. Hence, we observe pulses in excitable media and not fronts.

The Barkley model is a variant of the class of two-component Fitzhugh–Nagumo models. In the traditional Fitzhugh–Nagumo models $\mathcal{F}(u,v)$ in Eq. (1) is replaced by $\mathcal{F}_{\mathrm{FN}}(u,v)=u(1-u)(u-u_s)-v$. Thus, the nullclines $\mathcal{F}(u,v)=0$, which in the traditional Fitzhugh–Nagumo models are cubic polynomials, are replaced by straight lines in the Barkley model. Most of the qualitative behavior in the relevant parameter ranges is unchanged by this. Whereas the Barkley model is computationally more efficient and also analytically better tractable, the traditional Fitzhugh–Nagumo models display a feature which makes them more realistic for the description of excitable media in biology: the activator experiences an undershoot below its equilibrium value and slow decay in the tail region of a pulse. We expect that for the phenomena discussed in this paper the difference only leads to quantitative changes (indeed, we have done some tests to verify this assertion).

In order to study pulse propagation in 1D it is useful to first consider the case of constant v. The resulting bistable model is exactly solvable[19] and the pulse velocity is $c_f(v)=\sqrt{D/2}[1-2(u_s+v)]$. Hence, excitability requires that u_s is below the stall value $\frac{1}{2}$. The quantity $\Delta=\frac{1}{2}-u_s$ characterizes the strength of excitability and $c_f(0)$ coincides with the solitary pulse velocity for $\epsilon\to 0$.

Clearly, for $u_s<u_c=\frac{1}{2}$ and not too large a, pulse propagation fails for ϵ larger than some ϵ_c. The critical growth factor ϵ_c describes the onset of a saddle-node bifurcation.[11,13] The saddle node can be intuitively understood when we consider the activator pulse as a heat source, not unlike a fire-front in a bushfire. Due to the inhibitor the width of the pulse decreases with increasing ϵ. Hence, the heat contained within the pulse decreases. At a critical width, or a critical ϵ, the heat contained within the pulse is too small to ignite/excite the medium in front of the pulse.

For periodic wave trains the saddle node depends on the wavelength. The pulses run into the inhibitor field of their respective preceding pulse. Hence, propagation failure for periodic wave trains is controlled by the decay of the inhibitor and propagation is only possible when the interpulse distance L becomes larger than a critical wavelength L_c. Note that L_c diverges for $a\to 0$ when the decay rate of the inhibitor σ_2 vanishes.

In previous analytic works on one-dimensional pulses the limit of small ϵ was considered.[11,13] Then the solution of the activator u is well separated in two flat plateau regions with $u\approx 1$ and $u=0$ which are separated by a steep narrow front. This approach does not capture the square-root behavior of $c_0(\epsilon)$ close to the saddle-node bifurcation point. Close to the bifurcation point the solution resembles rather a bell-shaped pulse than a plateau. In this paper we will be concerned with the behavior near the bifurcation at ϵ_c and make explicit use of the observed bell-shape form of the solution. This allows us to describe the scaling behavior close to the bifurcation in terms of the equation parameters.

In two dimensions spiral waves are observed. Spirals can be created in excitable media from a finger, i.e., a 1D pulse which is extended in the second dimension and has one free end. Fingers may be created due to inhomogeneities in the excitability of the system.[20] At long times, the free end will either sprout or retract depending on the growing velocity c_g being positive or negative. If $c_g>0$, the tip of the finger will sprout into the fresh medium, and in particular it sprouts and curves backwards. This causes a nonvanishing curvature at the tip of the finger. Due to the increased curvature the finger tip is slower than the flat part of the front further away from the tip. Thus, the extending part far from the tip will curl up. This leads to the formation of a spiral with the free end at its core. The criterion $c_g>0$ is therefore a necessary criterion for spiral formation.

The transition to retraction always occurs before the 1D propagation failure. It is harder to tackle analytically. General and universal dynamical system approaches exploiting only the Euclidean symmetry of excitable media describe the transition as a drift bifurcation. These model independent theories give an explanation for the divergence of the core radius at the bifurcation point and also explain why a finger at the bifurcation point is translating with finite speed, i.e., that the transition to retracting fingers always occurs before the 1D propagation failure.[17] Unfortunately, it has the unphysical result that at the bifurcation point ϵ_g a spiral changes its sense of rotation.[17] Whereas these theories treat the spiral as a global solution of the underlying equations and see the transition to spiral waves as a pitchfork or drift bifurcation,[16,17] we take a local approach and describe the transition not as a bifurcation but as a quantitative change in the velocity of the finger, analogous to a Maxwell point in a first-order phase transition. Asymptotic techniques in the limit $\epsilon\ll 1$ have also been performed for this problem[14,15] and produced an analytical expression for the onset of retraction for small ϵ. Moreover, the authors were able to go one step further, in a detailed and sophisticated asymptotic analysis, and described the onset of meandering. In this paper we go beyond the restriction of small ϵ and propose a more intuitive approach to the problem of the growing velocity which nevertheless gives good agreement with the numerics.

In the following we assume given excitability parameters a, u_s and take ϵ as the bifurcation parameter. We will be looking for solutions that move with velocity c_0 in the x direction and may grow (or retract) with velocity c_g in the y direction. Thus, we rewrite Eqs. (1) in a frame moving with velocity (c_0, c_g) as

$$D(\partial_x^2+\partial_y^2)u+c_0\partial_x u+c_g\partial_y u+\mathcal{F}(u,v)=0, \qquad (2)$$

$$c_0\partial_x v + c_g\partial_y v + \epsilon(u - av) = 0. \tag{3}$$

II. PULSE PROPAGATION IN ONE-DIMENSIONAL EXCITABLE MEDIA

We first look for pulse and wave train solutions that do not depend on y. The reason for the failure to describe the pulse properties at ϵ_c within the framework of asymptotics employing the smallness of ϵ is due to the fact that at ϵ_c the pulse shape for u cannot be separated into a steep narrow front and a flat plateau. Hence, asymptotic techniques such as inner and outer expansions are bound to fail. Instead the pulse has the shape of a rather symmetric bell-shaped function (see Fig. 1). In the following we make explicit use of the shape of the pulse close to the critical point and parametrize the pulse appropriately; a method reminiscent of the method of collective coordinates in the studies of solitary waves.[21]

We choose u of the general form

$$u(x) = f_0 U(\eta) \quad \text{with} \quad \eta = wx, \tag{4}$$

where $U(\eta)$ is chosen as a symmetric, bell-shaped function, for example a Gaussian, of unit width and height. Hence, we restrict the solutions to a subspace of bell-shaped functions $U(\eta)$ which is parametrized by the amplitude f_0 and the inverse pulse width w. The aim of our method is to determine the so far undetermined parameters. This is done by minimizing the error made by the restriction to the subspace defined by Eq. (4).

We avoid further uncontrolled approximations and solve for the inhibitor field v explicitly

$$v(\eta) = f_0 \Theta V(\eta) \quad \text{with}$$

$$V(\eta) = e^{a\Theta\eta}\left[V^\star - \int_{L/2\,w}^{\eta} d\eta'\, e^{-a\Theta\eta'} U(\eta') \right], \tag{5}$$

where

$$\Theta = \epsilon/(c_0 w). \tag{6}$$

$V^\star$ is determined via the periodic boundary condition $v(-wL/2) = v(wL/2)$ and is

$$V^\star = \frac{1}{2\sinh\left(a\Theta \frac{L}{2} w \right)} \int_{-L/2\,w}^{L/2w} d\eta'\, e^{a\Theta(\eta' - L/2\,w)} U(\eta'). \tag{7}$$

We assume that the width w^{-1} is small compared to the distance between two consecutive pulses L. in the temporal domain this means that the time scale for the decay of the inhibitor is much longer than the activator pulse width. This assures that the activator field of consecutive pulses is well separated and only the inhibitor field overlaps, and that the interaction between pulses is mediated only through the inhibitor. Otherwise we would have to choose periodic functions $U(\eta)$. However, in this case we can now replace the limits of integration $\pm(L/2)w$ by $\pm\infty$. For the isolated pulse, i.e., when $L \to \infty$, $V^\star$ vanishes.

We now determine the parameters f_0 and w by projecting Eq. (2) onto the tangent space of the restricted subspace defined by Eq. (4). The tangent space is spanned by $\partial u/\partial f_0 = U$ and $\partial u/\partial w = \eta U_\eta$. This assures that the error made by restricting the solution space to the test functions is minimized. To achieve this, we multiply Eq. (2) with the basis functions of the tangent-space U and ηU_η, integrate over the η domain and require the projection to vanish, i.e.,

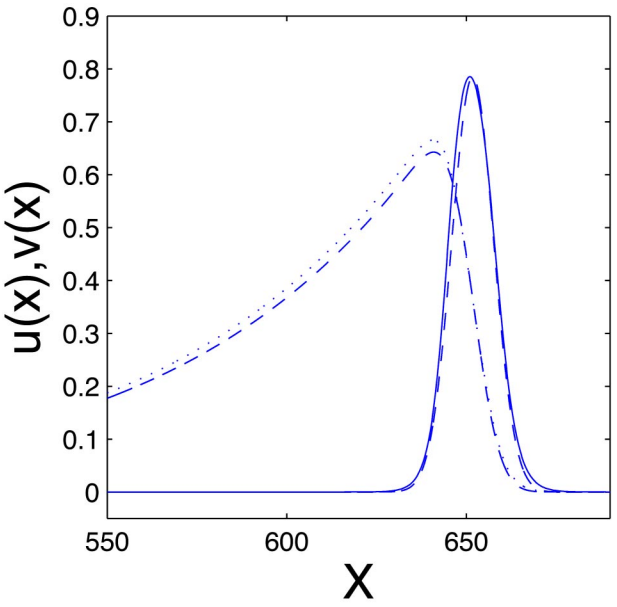

FIG. 1. Activator field u of a steady front with $\epsilon \approx \epsilon_c$ at $\epsilon = 0.0485$. The points depict the solution obtained by numerically integrating Eqs. (1). The continuous line is the theoretical curve obtained with the test function approach. Note that here ϵ is not even very close to $\epsilon_c \approx 0.049$.

$$\langle Dw^2 u_{\eta\eta} + u(1-u)(u - u_s - v) | U \rangle_{u = f_0 U(\eta)} = 0, \tag{8}$$

$$\langle Dw^2 u_{\eta\eta} + u(1-u)(u - u_s - v) | \eta U' \rangle_{u = f_0 U(\eta)} = 0, \tag{9}$$

where the brackets indicate integration over the whole η domain. The terms proportional to the velocity c_0 vanish.

The resulting equations can be combined to give, at fixed Θ and a, a quadratic equation for f_0 with two solutions $f_{0\pm}$ which describe the stable and unstable branch, respectively (see later for a subtle issue at the saddle node). We obtain

$$Af_0^2 + Bf_0 + C = 0, \tag{10}$$

where

$$A = \frac{3}{4}\langle U^4 \rangle - \frac{5\Theta}{6}\langle U^3 V \rangle - \frac{a\Theta^2}{3}\langle \eta U^3 V \rangle,$$

$$B = -\frac{5}{6}(1 + u_s)\langle U^3 \rangle + \Theta\langle U^2 V \rangle + \frac{a\Theta^2}{2}\langle \eta U^2 V \rangle,$$

$$C = u_s \langle U^2 \rangle. \tag{11}$$

The corresponding inverse width parameters $w_\pm$ for the stable and unstable branch are given by

$$w^2 = \frac{1}{D\langle U_\eta^2 \rangle}\{ f_0^2[-\langle U^4 \rangle + \Theta\langle U^3 V \rangle] + f_0[(1 + u_s)\langle U^3 \rangle - \Theta\langle U^2 V \rangle] - u_s \langle U^2 \rangle \}. \tag{12}$$

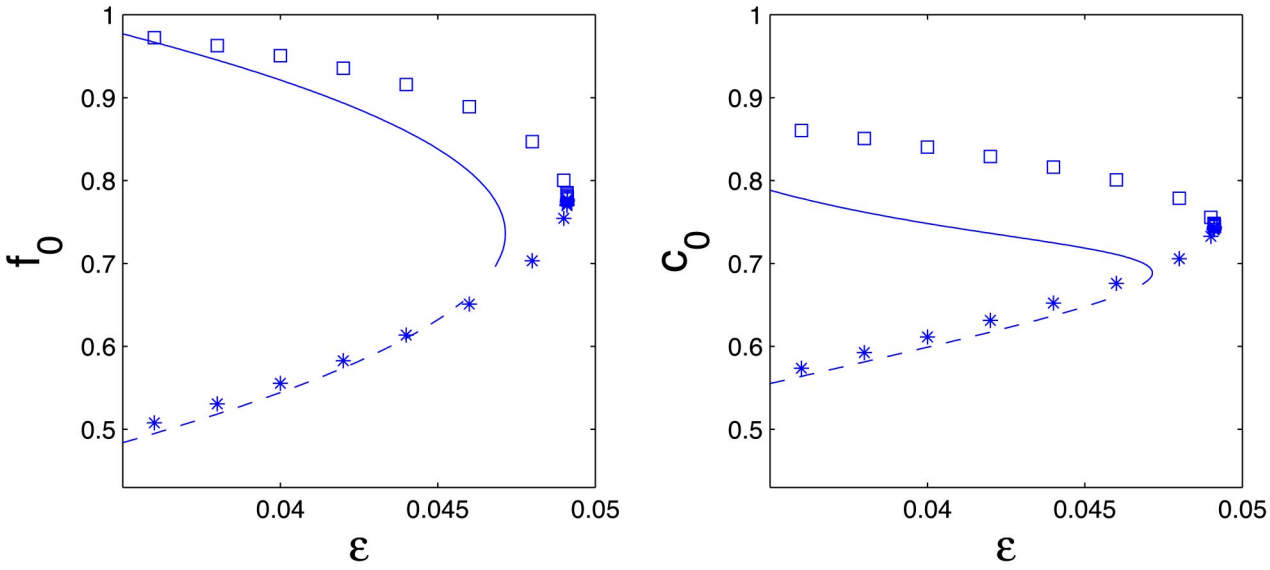

FIG. 2. (a) Amplitude f_0 as a function of ϵ. (b) Velocity c_0 as a function of ϵ. The parameters used were $D=3.0$, $a=0.22$, and $u_s=0.1$. The crosses depict the numerically obtained values of integrating the full system Eqs. (2) and (3), the lines depict the stable and unstable branch calculated with the test function approach, i.e., by using Eqs. (10), (12), and (13).

The velocity c_0 can now be determined in the standard way by multiplying Eq. (2) by u_x and integrating over x. We obtain

$$c_0=\frac{\int_{-\infty}^{\infty}\mathcal{F}(u,v)u_x dx}{\int_{-\infty}^{\infty}u_x^2 dx} =-\frac{f_0\Theta}{w\langle U_\eta^2\rangle}\left[\frac{f_0}{3}(\langle U^4\rangle-a\Theta\langle U^3V\rangle)-\frac{1}{2}(\langle U^3\rangle -a\Theta\langle U^2V\rangle)\right]. \tag{13}$$

Finally, we can determine ϵ from $\epsilon=c_0 w\Theta$. Multiplying Eq. (13) by w one sees that ϵ can be computed without calculating w and c_0.

We will use a Gaussian $U=e^{-\eta^2}$ as an ansatz function (4). Note that other symmetric bell-shaped functions such as a *sech*-function, are possible, too. Then one has $\langle U^n\rangle=\sqrt{\pi/n}$ and $\langle U_\eta^2\rangle=\langle U^2\rangle=\sqrt{\pi/2}$. The parameters of the test function f_0 and w, and the front velocity c_0 can now be determined numerically using Eqs. (10), (12), and (13).

Simplifications are possible in the useful limit $\Theta a\ll 1$. In this limit the (temporal) inverse pulse width $(w_n c_n)^{-1}$ is small compared to the inhibitor decay time $(\epsilon a)^{-1}$ [see definition of Eq. (6)]. Then in Eqs. (11) and (13) the terms proportional to a can be omitted, and for the calculation of $\langle U^nV\rangle$ one can omit the exponentials in Refs. 5 and 7 leading to

$$V(\eta)=V_s-\int_0^\eta U(\eta')d\eta', \quad V_s=\frac{\sqrt{\pi}}{2}\coth\left(\frac{a\epsilon L}{2c_0}\right). \tag{14}$$

Note that $V_s=\sqrt{\pi}/2$ corresponds to $V^\star=0$ [see Eq. 5] for small a. Now V can be replaced by the constant V_s in $\langle U^nV\rangle$ (the rest is an odd function) leading to

$$A=\sqrt{\pi}\left(\frac{3}{8}-\frac{5}{6\sqrt{3}}\Theta V_s\right),$$

$$B=\sqrt{\pi}\left[-\frac{5}{6\sqrt{3}}(1+u_s)+\frac{1}{\sqrt{2}}\Theta V_s\right], \quad C=\sqrt{\frac{\pi}{2}}u_s, \tag{15}$$

and from Eq. (13) we infer

$$\epsilon=\Theta^2 f_0\frac{1}{\sqrt{6}}\left(1-\frac{1}{\sqrt{3}}f_0\right). \tag{16}$$

A. Isolated pulses

We consider now isolated pulses for which the wavelength L is large compared to the decay length of the inhibitor $1/(\epsilon a)$. In Figs. 1 and 2 we show a comparison of our results Eqs. (10), (12), and (13) for f_0, w, and c_0, with a direct numerical simulation of Eqs. (1). The pulse shape, the critical bifurcation point ϵ_c, and the behavior near the saddle-node bifurcation of the amplitude $f_0(\epsilon)$ and of the velocity $c_0(\epsilon)$ are very well recovered. Note the square-root behavior near the saddle node.

Let us discuss some systematic features of the isolated pulses at criticality depending on the equation parameters a and u_s, which can be extracted from our approach. Solutions f_0 of Eq. (10) exist when the discriminant B^2-4AC is positive. The amplitude at the saddle node f_c is determined by the condition $B^2-4AC=0$. The corresponding bifurcation parameter ϵ_c can then subsequently be determined using Eqs. (12) and (13). Note that the saddle node, which occurs at the maximal bifurcation parameter ϵ_c, is not given by the relation $B^2-4AC=0$ since the condition of maximal ϵ is different from that of maximal Θ [see for example Eq. (16)]. In Fig. 3 we show ϵ_c and the corresponding amplitude at the saddle node f_c as a function of u_s for $a=0$ (continuous line)

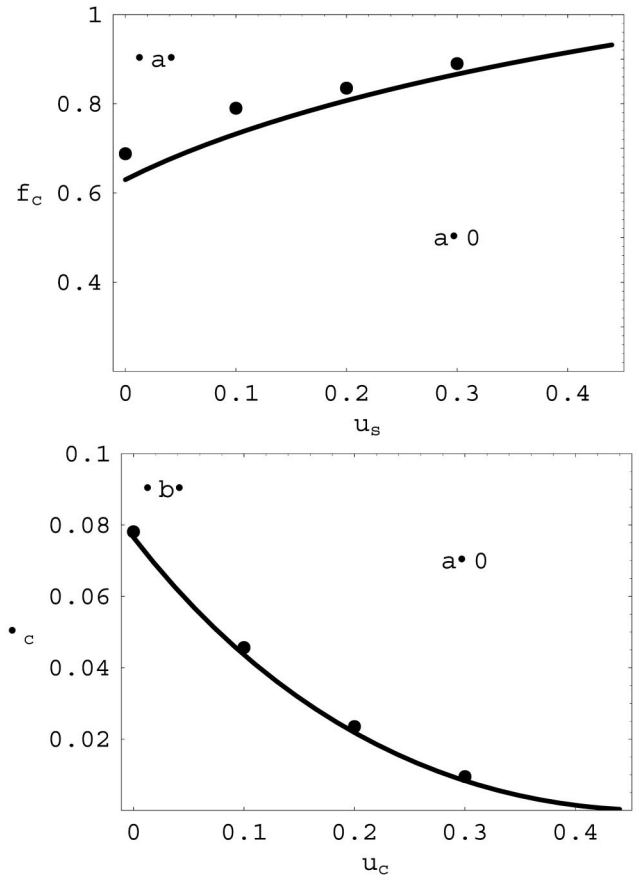

FIG. 3. Behavior at the saddle node of an isolated pulse for $a=0$. (a) The critical f_c vs u_s. (b) Critical amplitude ϵ_c vs u_s. Points correspond to simulations of the full one-dimensional version of Eqs. (2) and (3). The continuous line corresponds to the test function approach.

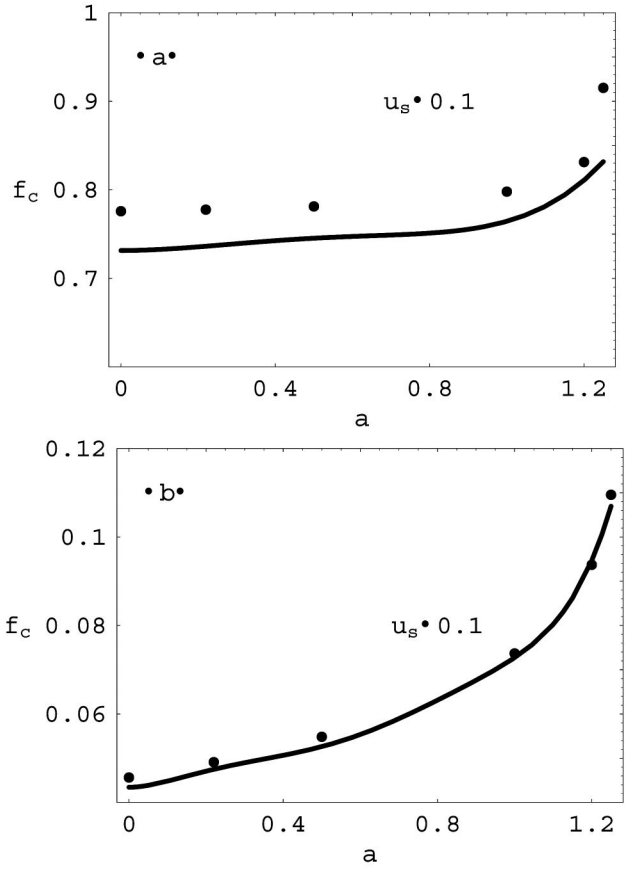

FIG. 4. Behavior at the saddle node of an isolated pulse for $u_s=0.1$. (a) The critical ϵ_c vs a. (b) Critical amplitude f_c vs a. Points correspond to simulations of the full one-dimensional version of Eqs. (2) and (3). The continuous line corresponds to the test function approach.

for the isolated pulse with $V_s=\sqrt{\pi}/2$. The points are results from a full solution of the one-dimensional version of the ordinary differential equations (ODEs) [Eqs. (2) and (3)]. In our approximation the limit of excitability (that is the maximum of u_s for which $\epsilon_c \to 0$) is $u_c=\sqrt{2}(81-50/\sqrt{2}-9\sqrt{81-50\sqrt{2}})/50=0.4745$, which is close to the exact stall-value $u_c=0.5$. Note that u_c is independent of a, as it should. Note also that pulse propagation in the neutrally stable case $u_s=0$ is possible. Moreover, pulses are supported even for negative u_s which we have checked numerically. We mention that for this calculation it is crucial to take into account the difference between maximizing ϵ and maximizing θ.

In Fig. 4 we show ϵ_c and f_c as functions of a for $u_s=0.1$. We see that our approximation (continuous line) reproduces all features of the ODEs (points). Figure 4 reveals that around $a=1.3$ the saddle-node bifurcation ceases to exist. The velocity c_0 approaches zero for these values. This correlates well with the fact that in the full system pulses become delocalized around $a=1.25$, i.e., front and tail of a pulse separate creating a domain with $u=1$, $v=1/a$, which represents a locally stable stationary state of the system. As a matter of fact, the inverse pulse width w diverges here for the test function approach.

B. Periodic wave trains

Even if a given set of equation parameters allows for propagation of a single solitary pulse, the system may not necessarily support a wave train consisting of several of such pulses. As a matter of fact, if the distance L between two consecutive pulses of the train becomes too small, the pulses run into the refractory tail of the preceding pulse and consecutively decay. The critical wavelength L_c is a lower bound for the wavelength for the existence of periodic wave trains. On can also think of keeping L fixed and, as before, vary ϵ. Then the saddle node $\epsilon_c(L)$ is a monotonically increasing function.

One can calculate L_c (or ϵ_c) essentially as before, except for the complication that due to V_s [Eq. (14)], the expressions for f_0, w and c_0, Eqs. (A4), (12), and (A7), cannot be cast in closed form depending only on θ. This is true even in the limit of small a. However, given the equation parameters ϵ, a, and u_s one may obtain L_c numerically as a consistency relation requiring that at each L there exists a $\tilde{\Theta}=1/(c_0 w)$ so that the value for c_0 obtained by solving Eqs. (10) and (12) and using the relation $c_0=\tilde{\Theta}/w$, matches the value for c_0 obtained by solving Eq. (13). We obtain very good agreement between our test function approach and the numerically obtained values for the critical wavelength L_c. In Fig. 5 we show a comparison of the values obtained by integrating the

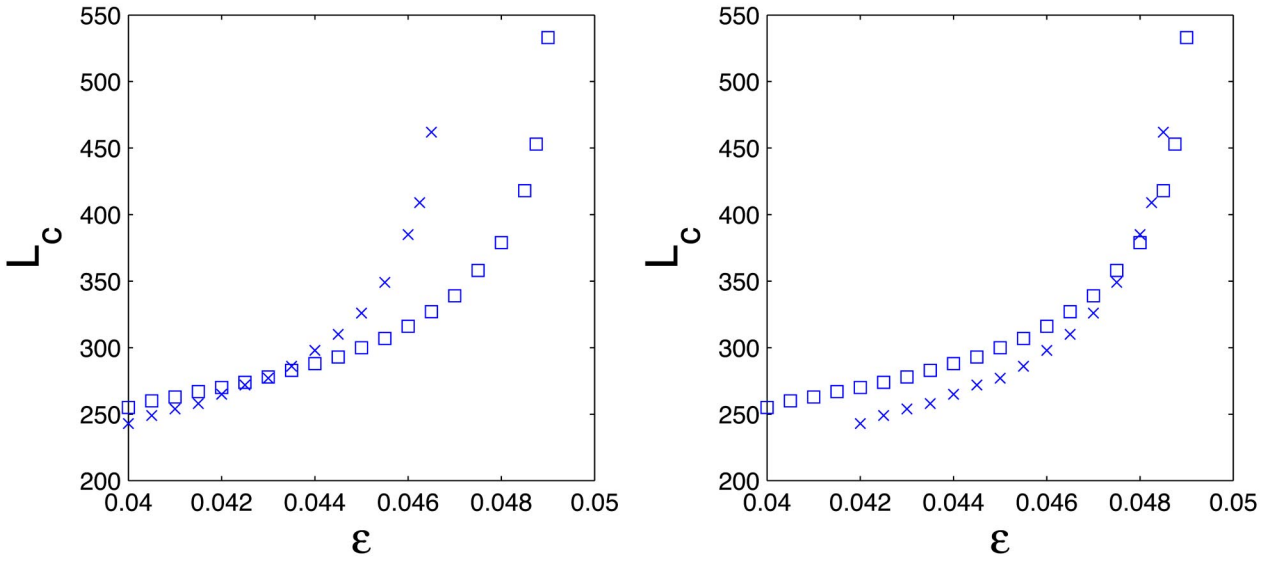

FIG. 5. (a) The critical wavelength L_c as a function of ϵ. Crosses depict the values obtained by direct simulation of the full system Eqs. (2) and (3). Squares depict the values obtained by the test function approach described in Sec. III. Parameters are again $D=3.0$, $a=0.22$, and $u_s=0.1$. In (b) the same numerical results as in (a) are presented but here the data points corresponding to the test-function approach are shifted along the ϵ axis such that the saddle nodes at $L_c=\infty$ (see Fig. 2), coincide.

full system Eqs. (2) and (3) with the calculation of the test function approach as described earlier. The critical wavelength L_c diverges when ϵ approaches ϵ_c where the saddle node of the localized pulse (i.e., $L=\infty$) causes propagation failure of isolated pulses (see Sec. II A and Fig. 2).

In the remainder of this section we will discuss the limit of large values of L, i.e., small perturbations to the saddle node ϵ_c of the isolated pulse. This causes small shifts of the critical ϵ, the amplitude f_0, and velocity c_0 when compared to their respective values in the case of isolated pulses and $L=\infty$. For simplicity, we restrict the calculation to the particular limit of small a.

We write

$$V_s=\frac{\sqrt{\pi}}{2}\sqrt{1+r},\quad r=\sinh^{-2}\left(\frac{a\epsilon L}{2c_0}\right)\approx 4\exp(-a\epsilon L/c_0) \tag{17}$$

and expand in terms of small r. The correction to the isolated pulse r is connected to the exponential tail of the inhibitor from the previous pulse. It thus captures the interaction between pulses mediated by the inhibitor. At leading order the shift with respect to the case $L=\infty$ of ϵ_c, f_0, and c_0 at the saddle node must be proportional to r. For small a one finds at leading order

$$[\epsilon_c(\infty)-\epsilon_c(L)]/\epsilon_c(\infty)=r=\gamma\exp(-a\epsilon L/c_0),\quad \gamma=4. \tag{18}$$

To see this note that the parameters f_0, w, c_0 are entirely given as a function of $R:=\Theta V_s$ via Eqs. (10), (12), and (13). Hence, if we multiply Eq. (16) by V_s^2, we have four equations to determine the parameters f_0, w, c_0, and R. We expand f_0, R, and ϵ_c with respect to r around the solutions of the isolated pulse. In particular, we write $\epsilon_c(L)=\epsilon_c(\infty)+r\epsilon_1$. The first-order correction ϵ_1 can be entirely determined using

$$\coth^2\frac{a\epsilon L}{2c}\,\epsilon=R^2 f\frac{1}{\sqrt{6}}\left[1-\frac{1}{\sqrt{3}}f\right], \tag{19}$$

where we deliberately ignored the subscripts to denote that f and c need to be expanded in r. The saddle-node condition $d\epsilon/df=0$ implies that the derivative of the right-hand side of Eq. (19) with respect to f vanishes at $r=0$, and we obtain the first-order correction ϵ_1 leading to Eq. (18). This result is confirmed by our numerical simulations. We have determined the shift of ϵ_c due to finite wave length L for $a\to 0$ and $u_s=0.1$ numerically from the ODEs and find $\gamma=4.3$. This shows the accuracy of our test function approach for the saddle node shift. The leading-order approximation for the saddle node behavior is good down to about $aL=40$. For $a=0.22$ we find numerically $\gamma=5.5$.

In Sec. IV we will touch on some questions of stability of the wave train solutions near the saddle node.

III. GROWING VELOCITY AND RETRACTING FINGERS IN TWO-DIMENSIONAL EXCITABLE MEDIA

In this section we develop a two-dimensional extension of the test function approach. We study isolated finger solutions, i.e., solutions which in the $-y$ direction go over into an isolated pulse (moving with velocity c_0 in the x direction) and rapidly decay to zero in the $+y$ direction. In the y coordinate they may be regarded as fronts, which grow or retract with velocity c_g (see Fig. 6 for a retracting case). We derive an explicit formula for the growing velocity c_g. We now investigate the full two-dimensional system (2) and (3) in a frame moving with velocity (c_0, c_g).

We introduce a product ansatz for the activator field

$$u(x,y)=f(y)U(\eta) \tag{20}$$

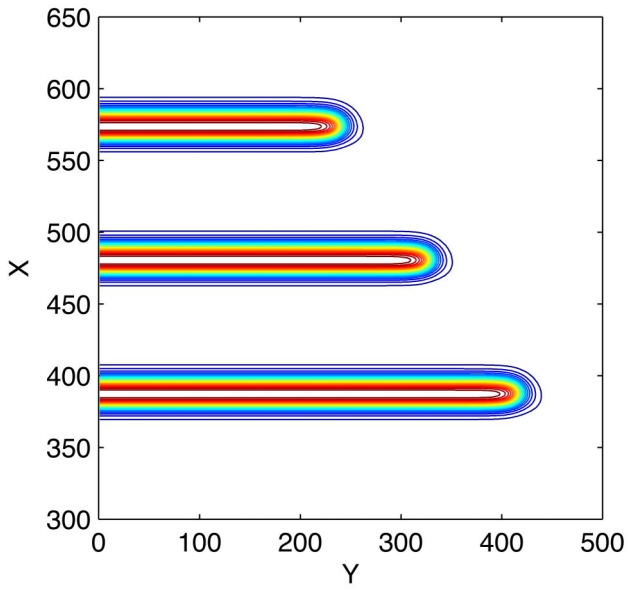

FIG. 6. Contour plot of the activator u of a retracting finger at different times.

with test function $U(\eta)$. This approximation neglects possible curvature at the tip. Again, we avoid any further uncontrolled approximation and solve for $f(y)$ and $v(x,y)$ in a systematic way. Note that $f(y)$ replaces the constant f_0 in Eq. (4). The solution of Eq. (3) with the ansatz Eq. (20) can be written explicitly as

$$v(\eta,y) = -\Theta \int_{\infty}^{\eta} e^{a\Theta(\eta-s)} f\left\{\frac{1}{\Delta}\left[\frac{c_g}{c_0 w}(s-\eta)+y\Delta\right]\right\} \times U\left\{\frac{1}{\Delta}\left[s+\left(\frac{c_g}{c_0 w}\right)^2 \eta\right]\right\} ds, \tag{21}$$

where $\Delta = 1+(c_g/c_0 w)^2$. Further calculations with this full expression appear prohibitive. Since we are mainly interested in the reversal point of c_g we resort to an (asymptotic) expansion in powers of c_g, restricting ourselves here to the first two terms. From Eq. (21) one obtains

$$v(\eta,y) = \Theta[g_0(y)V_0(\eta) + c_g g_1(y) V_1(\eta) + \mathcal{O}(c_g^2)], \tag{22}$$

where

$$g_0(y) = f(y) \quad \text{and} \quad g_1(y) = f'(y). \tag{23}$$

$V_0(\eta)$ coincides with $V(\eta)$ of Eq. (5) with $V^\star = 0$ and $L = \infty$ [or, for small a, with Eq. (14)] and

$$V_1(\eta) = -\frac{1}{c_0 w} e^{a\Theta\eta} \int_{\infty}^{\eta} e^{-a\Theta\eta'} V_0(\eta')\, d\eta'. \tag{24}$$

Note that the first-order correction of the inhibitor Eq. (24) can also be obtained by inserting the ansatz Eq. (22) into Eq. (3) and solving for successive orders of c_g.

Repeating the procedure that led to Eq. (8) for f_0, i.e., multiplying Eq. (2) with $U(\eta)$ and integrating over η, we obtain using Eq. (23)

$$Df'' + c_g f' + F(y) f = 0 \tag{25}$$

with

$$F(y) = \{-Dw^2\langle U_\eta^2\rangle + \langle U^2[1-f(y)U][f(y)U - \Theta[f(y)V_0 + c_g f'(y) V_1] - u_s]\rangle\}/\langle U^2\rangle. \tag{26}$$

Note that for $f(y) \equiv f_{0\pm}$, where $f_{0\pm}$ are the solutions of the quadratic Eq. (10), we have $F(y) = 0$.

We first neglect the higher-order correction of the inhibitor field $V_1(y)$. Then F is a quadratic form in $f(y)$ with zeros $f_{0\pm}$, and Eq. (25) can be solved exactly with the ansatz

$$f'(y) = \alpha f(f - f_0), \tag{27}$$

which states that far away from the tip $f(y)$ is constant and takes values 0 or f_0. The constant of proportionality α can be determined. Using Eq. (27) we obtain for the growing velocity

$$c_{g0} = \sqrt{\frac{D}{2}} \sqrt{\frac{\langle U^4\rangle - \Theta\langle U^3 V\rangle}{\langle U^2\rangle}} (f_{0+} - 2 f_{0-}). \tag{28}$$

The point $c_{g0} = 0$ is fixed by the condition $f_{0+} = 2 f_{0-}$. The value for ϵ where $c_{g0} = 0$ which we denote by ϵ_g, matches very well the value obtained by numerically integrating the full two-dimensional system Eqs. (2) and (3). However, the behavior for nonzero growing velocities is not captured by Eq. (28). In fact, the slope $\partial c_{g0}/\partial\epsilon$ close to the reversal point is too small by an order of magnitude for the parameters used in Figs. 1, 2, 5, and 6 when compared to the values obtained by the full two-dimensional simulation.

To obtain the correct slope we need to take into account the correction $V_1(\eta)$ of the inhibitor field. Including the first-order correction $V_1(\eta)$ in Eq. (25) we solve for c_g analogously to the determination of c_0 in Sec. II by multiplying Eq. (25) by $f'(y)$ and subsequently integrating over y. To $\mathcal{O}(c_g)$ we obtain

$$c_g = c_{g0} \frac{1}{1 + \frac{1}{2} G_0 f_0 + \frac{3}{10} G_1 f_0^2}, \tag{29}$$

where

$$G_0 = -\Theta \frac{\langle U^2 V_1\rangle}{\langle U^2\rangle} \quad \text{and} \quad G_1 = \Theta \frac{\langle U^3 V_1\rangle}{\langle U^2\rangle}. \tag{30}$$

As expected the higher-order corrections G_0 and G_1 do not change the value of ϵ_g, but change the slope of $\partial c_g/\partial\epsilon$. In Fig. 7 we show a comparison of the test function approach and of Eq. (29) with numerically obtained data. The correspondence close to $c_g = 0$ is striking. To obtain better agreement further away from $c_g = 0$ one would have to include higher-order terms in expression (22).

IV. SUMMARY AND DISCUSSION

We have developed a nonperturbative method to study critical wave propagation of single pulses and periodic wave trains in one and two dimensions. The method is based on the observation that near the bifurcation point the pulse shape is close to a symmetric bell-shaped function. A test function approximation, optimizing the two free parameters

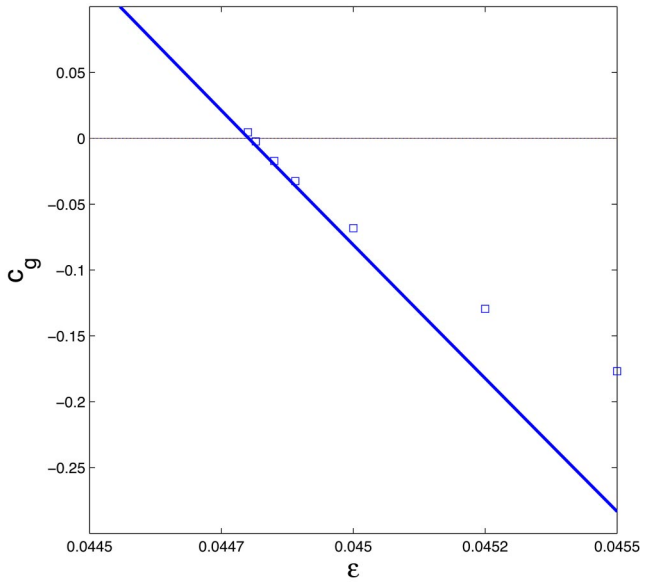

FIG. 7. Growing velocity c_g as a function of ϵ. The crosses depict the values obtained by direct numerical integration of Eqs. (2) and (3). The continuous line shows the theoretical curve Eq. (29) using the test function approach of Sec. IV A. We have shifted the curve along the ϵ axis by the difference of the ϵ values $\Delta\epsilon = 0.001\,972$ for the saddle nodes obtained by the numerical simulations of the full system Eqs. (2) and (3), and the test function approach of Sec. II.

of a bell-shaped function, i.e., amplitude and width, allows to calculate the wave speed of a critical and close-to-critical pulse. We were able to study propagation failure of isolated pulses and wave trains, and moreover the test is capable of capturing more general features such as the transition from excitability to bistability. We have also performed our test function method with a more general class of nonsymmetric test functions to calculate the pulse parameters and velocities. It turns out that near the saddle node the asymmetry indeed becomes irrelevant.

We extended our method to two-dimensional situations, and used it to study broken fronts. Depending on parameters these fingers may either retract or sprout and start spiraling. We studied the growing velocity of a critical finger whose growing velocity is close to zero. Our test function method combined with a separation ansatz for the two-dimensional finger tip yields analytical expressions for the growing velocity which depend only on the equation parameters and which are for large parameter ranges in good agreement with the numerically obtained values. We elaborated on the importance of the inhibitor field for the growing velocity.

Let us finally mention an interesting observation for one-dimensional wave trains. Below some (rather large) pulse separation (wavelength) the wave train looses stability not via a saddle node but via a Hopf bifurcation. This may be seen in numerical simulations of the full system Eqs. (2) and (3) (and also of other excitable media equations such as the Fitzhugh–Nagumo equation) and in analytical approximations, either based on a time-dependent generalization of the test function approach or on a systematic reduction scheme valid near the saddle node. At the codimension two point where the saddle node of the wave train coincides with the Hopf bifurcation the Hopf frequency becomes infinite. This time-dependent phenomenon can of course not be captured within the current stationary algebraic framework. This phenomenon and its implications will be published separately. For completeness we have included a time-dependent extension of the test function approach which allows for Hopf bifurcation in the Appendix. This seems to be related to the phenomenon of alternans[7] which has been studied in a different parameter regime far away from the saddle node.[8]

Another interesting problem we plan to address is the selection of the wavelength (or pitch) of spirals. In simulations we found that near ϵ_g, where growth of fingers becomes small, the selected wavelength diverges. Kinematic theory[11,12,22,23] addresses this problem. Kinematic theory provides, in principle, a relationship between the rotation frequency of a spiral and its core radius. However, it fails to provide expressions for either of the two which only depend on the equation parameters. A connection of our theory with kinematic theory is planned for further research to fill this gap.

ACKNOWLEDGMENTS

The authors would like to thank the INLN where parts of this work were done for its hospitality. G.A.G. would like to thank Valentin Krinsky for introducing him to this research. The authors would like to thank Dwight Barkley, Gianne Derks, Alain Karma, Jim Keener, Ian Melbourne, Sasha Panfilov, Alain Pumir, Sebastian Reich, and Mark Roberts for valuable discussions. G.A.G. was partly supported by a European Commission Grant, Contract No. HPRN-CT-2000-00113, for the Research Training Network *Mechanics and Symmetry in Europe* (MASIE) and by an Australian Academy of Science Travel Grant. Part of the simulations were done with the XDim Interactive Simulation Package developed by P. Coullet and M. Monticelli, who L.K. thanks for their support.

APPENDIX: TIME-DEPENDENT SYSTEM FOR WAVE PROPAGATION OF PULSES AND PERIODIC WAVE TRAINS IN ONE-DIMENSIONAL EXCITABLE MEDIA

In this appendix we present the time-dependent calculation for our test function approach. For simplicity we restrict ourselves to small values of a. This means that the width of the activator pulse u is small compared to the width of the decaying inhibitor field v. We include now temporal dependency of the pulse variables f_0, c_0, and w. We study pulse trains and note that the localized pulse can be obtained in the limit $L \to \infty$. Hence, we choose u of the form

$$u(x) = \sum_0^N f_n(t) U(\eta_n). \tag{A1}$$

The sum extends over all N pulses. We defined $\eta_n = w_n(t) \times [x - \phi_n(t)]$ and $U(\eta)$ is chosen as a Gaussian $e^{-\eta^2}$ as earlier. We allow for individual dynamics of the pulses characterized by the amplitude $f_n(t)$, the inverse width $w_n(t)$, and the position $\phi_n(t)$. For a stationary wavetrain the f_n and w_n will be constant and all equal, and $\phi_n = n(c/L)t$, where c

is the velocity. We will restrict ourselves to the situation where the perturbations around such a state are small and slowly varying. We insert the ansatz Eq. (A1) into the general expression

$$v(t,x) = -\epsilon \int_{\infty}^{t} e^{-\epsilon a(t'-t)} u(t',x), dt'$$

obtained from the second Eq. (1). Assuming that the (temporal) inverse pulse width $(w_n c_n)^{-1}$ is small compared to the inhibitor decay time $(\epsilon a)^{-1}$, we obtain the following expression valid in the vicinity of the $n=0$ pulse, which is assumed to pass the origin at $t=0$

$$v(\eta_0) = \epsilon \frac{f_0}{w_0 c_0}\left[\frac{1}{2}\langle U\rangle - \int_0^{\eta} d\eta' U(\eta')\right] + \epsilon\langle U\rangle \sum_{l=1}^{\infty} e^{-l\epsilon a L/c_l} \frac{f_l}{w_l c_l} + s_0 \int_0^{\eta} d\eta'\, \eta' U(\eta'), \tag{A2}$$

where the brackets indicate integration over the whole η domain, and

$$s_0 = -\epsilon\{\partial_t[f_0/(c_0 w_0)]\}/(w_0 f_0). \tag{A3}$$

In order to determine f_n, w_n, and c_n we again project Eq. (2) onto $U(\eta)$, $\eta U'(\eta)$, and $U'(\eta)$. After combining the first two equations appropriately one obtains

$$\langle U^2\rangle\left(\frac{\dot f_0}{f_0} - \frac{\dot w_0}{w_0}\right) = -u_s\langle U^2\rangle + \frac{5}{6}(1+u_s)\langle U^3\rangle f_0 - \frac{3}{4}\langle U^4\rangle f_0^2 - \left(\langle U^2\rangle - \frac{5}{6}\langle U^3\rangle f_0\right) V_p - \left(\frac{5}{6}\langle U^3\rangle - \frac{3}{4}\langle U^4\rangle f_0\right)\frac{s_0}{2}, \tag{A4}$$

$$\langle U^2\rangle \frac{\dot w_0}{w_0} = 2D w_0^2 \langle U'^2\rangle + \frac{1}{3}(1+u_s)\langle U^3\rangle f_0 - \frac{1}{2}\langle U^4\rangle f_0^2 + \frac{1}{3}\langle U^3\rangle f_0 V_p - \left(\frac{1}{3}\langle U^3\rangle - \frac{1}{2}\langle U^4\rangle f_0\right)\frac{s_0}{2}, \tag{A5}$$

where

$$V_p = \epsilon\langle U_1\rangle\left(\frac{1}{2}\frac{f_0}{c_0 w_0} + \sum_{l=1}^{\infty} e^{-l\epsilon a L/c_l}\frac{f_l}{w_l c_l}\right). \tag{A6}$$

The third projection gives an algebraic relation

$$c_0 w_0 \langle U'^2\rangle = \frac{\epsilon f_0}{c_0 w_0}\left(\frac{1}{2}\langle U^3\rangle - \frac{f_0}{3}\langle U^4\rangle\right). \tag{A7}$$

These equations are written for the pulse $n=0$. They apply correspondingly to the other pulses.

First consider the case of a stationary, isolated pulse ($L=\infty$) where $s_0=0$ and the sum in Eq. (A6) vanishes. The resulting algebraic relations are easily solved, and correspond in the limit of $a\to 0$ to Eqs. (10), (12), and (13). With reasonable initial conditions, simulation of the ODEs Eqs. (A4), (A5), together with (A7) leads to the same result as described in Sec. II. The ODEs Eqs. (A4) and (A5) relax to the stationary values obtained in Sec. II.

This time-dependent test function approach allows to go beyond the stationary bifurcations discussed in Sec. IV. As mentioned in Sec. II the saddle-node bifurcation related to propagation failure for well separated pulses transforms into a subcritical Hopf bifurcation via a Takens–Bogdanov point when the pulse separation is reduced below a critical value L_c. This work will be published elsewhere. The Hopf bifurcation can be captured within the ODE system Eqs. (A4), (A5), and (A7), and some preliminary simulations have been done.

[1] A. T. Winfree, *When Time Breaks Down* (Princeton University Press, Princeton, NJ, 1987).
[2] J. M. Davidenko, A. M. Pertsov, R. Salomonsz, W. Baxter, and J. Jalife, Nature (London) **335**, 349 (1992).
[3] F. Siegert and C. Weijer, Physica D **49**, 224 (1991).
[4] M. Berridge, P. Lipp, and M. Bootman, Nature Reviews Molecular Cell Biology **1**, 11 (2000).
[5] A. T. Winfree, Science **266**, 175 (1972).
[6] See review articles in the focus issue Chaos **8** (1) (1998).
[7] J. B. Nolasco and R. W. Dahlen, J. Appl. Physiol. **25**, 191 (1968).
[8] A. Karma, Chaos **4**, 461 (1994).
[9] A. S. Mikhailov, *Foundations of Synergetics I: Distributed Active Systems*, 2nd ed. (Springer, Berlin, 1994).
[10] W. Jahnke and A. T. Winfree, Int. J. Bifurcation Chaos Appl. Sci. Eng. **1**, 445 (1991).
[11] V. S. Zykov, *Simulation of Wave Processes in Excitable Media* (Manchester University Press, New York, 1987).
[12] A. S. Mikhailov, V. A. Davydov, and V. S. Zykov, Physica D **70**, 1 (1994).
[13] E. Meron, Phys. Rep. **218** (1) (1992).
[14] V. Hakim and A. Karma, Phys. Rev. Lett. **79**, 665 (1997).
[15] V. Hakim and A. Karma, Phys. Rev. E **60**, 5073 (1999).
[16] D. Barkley and I. G. Kevrekidis, Chaos **4**, 453 (1994).
[17] P. Ashwin, I. Melbourne, and M. Nicol, Nonlinearity **12**, 741 (1999).
[18] D. Barkley, Physica D **49**, 61 (1991).
[19] J. Keener and J. Sneyd, *Mathematical Physiology* (Springer, New York, 1998).
[20] A. N. Reshetilov, A. M. Pertsov, and V. I. Krinsky, Biofizika **24**, 192 (1979).
[21] A. Scott, *Nonlinear Science—Emergence and Dynamics of Coherent Structures* (Oxford University Press, Oxford, 1999).
[22] W. K. Burton, N. Cabrera, and F. C. Franck, Philos. Trans. R. Soc. London, Ser. A **243**, 299 (1951).
[23] J. P. Tyson and J. P. Keener, Physica D **32**, 327 (1988).